

Electron transport through quantum wires and point contacts

P. Havu, M. J. Puska, and R. M. Nieminen

Laboratory of Physics, Helsinki University of Technology, P.O. Box 1100, FIN-02015 HUT, Finland

V. Havu

Institute of Mathematics, Helsinki University of Technology, P.O. Box 1100, FIN-02015 HUT, Finland

We have studied quantum wires using the Green's function technique and the density-functional theory, calculating the electronic structure and the conductance. All the numerics are implemented using the finite-element method with a high-order polynomial basis. For short wires, i.e. quantum point contacts, the zero-bias conductance shows, as a function of the gate voltage and at a finite temperature, a plateau at around $0.7G_0$. ($G_0 = 2e^2/h$ is the quantum conductance). The behavior, which is caused in our mean-field model by spontaneous spin polarization in the constriction, is reminiscent of the so-called 0.7-anomaly observed in experiments. In our model the temperature and the wire length affect the conductance-gate voltage curves in the same way as in the measured data.

73.21.Hb, 73.63.Nm

I. INTRODUCTION

Two-dimensional (2D) nanostructures can be fabricated at semiconductor interfaces (such as GaAs/AlGaAs), using lithographic techniques and gate electrodes [1–3]. In these structures conducting electrons form a quasi-2D electron gas at the interface. Doping impurities are separated from the 2D electron gas making the transport ballistic over the nanostructure. This enhances the importance of quantum mechanical effects.

An interesting 2D nanostructure is the quantum wire (QW), which is a laterally narrow electron pathway connecting two (infinite) electrodes. Because of the ballistic electron transport the conductance is quantized in units of the quantum $G_0 = 2e^2/h$. The 2D electron states are quantized in the direction perpendicular to the axis of the wire. Each occupied perpendicular state gives rise to one conducting mode adding one quantum to the conductance. In a typical measurement, the conductance is recorded as a function of the gate voltage which lowers the potential in the wire region, influencing its width or the average electron density. The increase in the number of conducting modes results in a staircase as a function of the gate voltage. Recently, Kane *et al.* [1] and Reilly *et al.* [4] have measured conductances of QW's with different geometries. The quantization of the conductance is clearly seen in the measurements.

A short quantum wire can be characterized as a quantum point contact (QPC). QPC's exhibit the so-called 0.7-anomaly which is a small plateau in conductance around $0.7-0.5 G_0$ as a function of the gate voltage [2]. The plateau moves from $0.7 G_0$ to $0.5 G_0$ as the electron density in the quantum wire is lowered or the QPC is in a strong magnetic field. The plateau becomes more pronounced when temperature increases from the milli-Kelvin region to a few Kelvin. At higher temperatures the anomaly disappears. The length of the wire affects also the anomaly [4] so that in long wires the anomaly is

around $0.5 G_0$ and in shorter ones around $0.7 G_0$. The measurements show a short plateau also within the next quantum step around $1.5 \dots 1.76 G_0$.

There are several different explanations for the 0.7 anomaly. One of them [5,6] is based on the Kondo model where an unpaired electron is localized at the QPC. In the ground state this electron is in the spin-singlet state with the scattering electrons from the leads. The spin coupling results in a high density of states, a Kondo resonance, at the Fermi level and thus in an enhanced conductance around zero bias voltage. This zero-bias anomaly is similar to the Kondo effect in single-electron transistors [7]. In the case of the QPC the Kondo model seemingly explains the plateaus and their behavior as a function of the temperature and the external magnetic field [5,6].

Another explanation is provided by the semi-empirical model by Reilly *et al.* [4]. In this model the plateau is caused by the local spin polarization of the electron gas at the QPC. For small electron densities at the QPC the polarization vanishes, but when the electron density is increased using the gate voltage a spin gap opens and causes the polarization. The opening of the spin-gap depends on the QPC configuration and temperature, and in different cases the conductance plateaus appear at different values. A spin-polarization model has also been presented by Berggren and Yakimenko [8]. They used the density-functional theory (DFT) to calculate the electron density in a quantum wire as function of the gate voltage. The conductance was calculated using the Büttiker model [9] with parameters obtained by fitting the effective DFT potential in the middle of the QW. Also Meir *et al.* [6] and Hirose *et al.* [5] reported DFT calculations for a QW in order to model the QPC resonance states needed in the Kondo model. Also recent measurements utilising the resonant interaction between coupled QW's show evidence of the formation of localized magnetic moment in a constriction of the 2D electron gas [10,11].

In this work we investigate the spontaneous spin-

polarization model for QW's. Our aim is to make within this model accurate and realistic calculations for the conductance, in order to study how far the model can describe the experimental findings. We use the DFT and the Green's functions techniques (see, for example Xue *et al.* [12]) to calculate the electron density and the conductance. For the electron spin densities the use of the Green's function technique is computationally more demanding than solving for the wave functions of a finite system. However, it has important advantages. First, an infinite system without any artificial periodicity can be treated. It is also possible to add the bias voltage between the electrodes and calculate the charge density and the current through the structure self-consistently. We solve for the DFT-Green's function equations numerically by the finite-element method using our recent implementation [13].

We use the effective atomic units which are derived by setting the fundamental constants $e = \hbar = m_e = 1$, and the material constants $m^* = \epsilon = 1$. m^* and ϵ are the relative effective electron mass and the relative dielectric constant respectively. The effective atomic units are transformed to the usual atomic and SI units with the relations

$$\begin{aligned} \text{Length: } 1 a_0^* &= 1 \frac{\epsilon}{m^*} a_0 \approx 10.0307 \text{ nm} \\ \text{Energy: } 1 \text{ Ha}^* &= 1 \frac{m^*}{\epsilon^2} \text{ Ha} \approx 11.3079 \text{ meV} \\ \text{Current: } 1 \text{ a.u.}^* &= 1 \frac{m^*}{\epsilon^2} \text{ a.u.} \approx 2.7512 \mu\text{A}. \end{aligned}$$

Above, the numbers on the right-hand side are obtained by using the parameters for GaAs, i.e. $m^* = 0.067$ and $\epsilon = 12.7$. They are used in illustrating our results. Ha denotes the Hartree energy unit.

II. MODEL AND THEORETICAL METHODS

Our strictly 2D model for a QW is shown in Fig. 1. We use a simplified geometry in order to see the effects due to different shapes of the wire. The calculation area, Ω , consists of the QW and some parts of the electrodes.

The semi-infinite electrodes consist of the positive background charge with the constant density of $0.2(a_0^*)^{-2} \approx 2 \times 10^{11} e/\text{cm}^2$ and the neutralizing 2D electron gas with the density $\rho(r)$.

At both sides of the electrodes and the wire we include some empty vacuum, and the electron density is required to vanish at the outer boundaries parallel to the wires.

The electron density at the axis of the electrode is then typical for GaAs/GaAlAs systems and the Fermi energy (the width of the occupied energy band) is $0.63 \text{ Ha} = 7.1 \text{ meV}$. The neutrality makes the calculation of the electrostatic potential in the self-consistent DFT calculations possible. The QW is also modeled using a rigid uniform positive background charge. We control the positive charge density ρ_j in the wire region Ω_{QW} (the darker area in Fig. 1) in order to mimic the effects

of a gate voltage. The denser the background charge the deeper the effective potential is, i.e.

$$V_g(r) = \int_{\Omega_{QW}} \frac{-\rho_j}{|r - r'|} dr', \quad (1)$$

where $r = \{r_x, r_y\}$ are the 2D coordinates. We calculate V_g at the midpoint of the wire and use this value as the gate voltage in our illustrations below. The dependence of the gate voltage can be written in the form

$$V_g = C_j \rho_j, \quad (2)$$

where the coefficient C_j depends on the shape of the wire. $C_j = 218 \text{ mV} a_0^{*2}$, $234 \text{ mV} a_0^{*2}$ and $248 \text{ mV} a_0^{*2}$ for wires with the width W of $5a_0^*$ and lengths L of $6a_0^*$, $7a_0^*$ and $8a_0^*$, respectively. In chapter III we denote these wires as D, E and F.

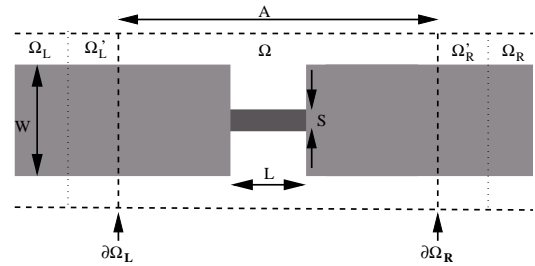


FIG. 1. 2D quantum wire between two electrodes. The gray areas denote the rigid positive background charge. The electrodes continue to the infinity outside the calculation region. The uniform background charge density is varied in the dark-gray wire region in order to model the effects of the gate voltage.

We use the DFT within the local density-approximation to calculate the electron density. In the self-consistent iterations the electron density is first calculated using Green's functions. The electron density is then used to calculate the effective potential V_{eff} as

$$V_{eff}(r) = \int_{\Omega + \Omega'_L + \Omega'_R} \frac{\rho(r') - \rho_+(r')}{|r - r'|} dr' + V_{xc}(r) + V_{bias}(r) \quad (3)$$

Above, the first term on the right-hand side is the Coulomb potential, computed as an integral and not from the Poisson equation because of the 2D calculation space. The electron density in the electrodes $\Omega_{L/R}$ is assumed to coincide with that in an infinite uniform wire. Then we can include the outside regions into the Coulomb integral within the buffer regions Ω'_L and Ω'_R which are large enough. For the exchange-correlation potential, V_{xc} , we use the 2D-LDA functional by Attaccalite *et al.* [14,15]. The potential V_{bias} is a linear ramp taking care of the boundary conditions under a finite bias so that the potential in the left electrode is shifted relative to that in the right electrode by a given bias voltage V_{SD} . The effective potential determines through the Green's functions a

new electron density and the procedure is repeated until convergence.

The retarded Green's function is obtained by solving the equation

$$(\omega + \frac{1}{2}\nabla^2 - V_{eff}(r))G^r(r, r'; \omega) = \delta(r - r'), \quad (4)$$

where ω is the electron energy. At the boundaries $\partial\Omega_{L/R}$ we use open boundary conditions given by the Dirichlet-to-Neumann map on the boundary. This means that there are no reflections. One can next calculate the so-called lesser Green's function, $G^<(r, r'; \omega)$. For zero bias, when the Fermi functions in the left and right electrodes are identical, i.e. $f_L(\omega) = f_R(\omega)$, $G^<$ is obtained as

$$G^<(r, r'; \omega) = 2f_{L/R}(\omega)G^r(r, r'; \omega). \quad (5)$$

In the non-equilibrium situation when $f_L(\omega) \neq f_R(\omega)$ we have

$$\begin{aligned} G^<(r, r'; \omega) = & -if_R(\omega) \int_{\partial\Omega_R} \int_{\partial\Omega_R} G^r(r, r_R; \omega) \Gamma_R(r_R, r'_R; \omega) \\ & \times G^a(r'_R, r'; \omega) dr_R dr'_R \\ & -if_L(\omega) \int_{\partial\Omega_L} \int_{\partial\Omega_L} G^r(r, r_L; \omega) \Gamma_L(r_L, r'_L; \omega) \\ & \times G^a(r'_L, r'; \omega) dr_L dr'_L. \end{aligned} \quad (6)$$

Above, $\Gamma_{L/R}$ are functions connecting the calculation area to the outside electrodes. They have nonzero values only on the boundaries $\partial\Omega_{L/R}$. The imaginary part of $G^<$ is related to the density of states, and the electron density is calculated by integrating over the energy

$$\rho(r) = \frac{-1}{2\pi} \int_{-\infty}^{\infty} \text{Im}(G^<(r, r; \omega)) d\omega. \quad (7)$$

The local density of states (LDOS) in the QW region is calculated as

$$g_{QW}(\omega) = \frac{-1}{2\pi} \int_{\Omega_{QW}} \text{Im}(G^<(r, r; \omega)) dr. \quad (8)$$

LDOS is a continuous function in our calculations and thus the finite-size effects are small.

The electron tunneling probability $T(\omega)$ is calculated as a function of the electron energy using the Green's functions as

$$\begin{aligned} T(\omega) = & \int_{\partial\Omega_L} \int_{\partial\Omega_L} \int_{\partial\Omega_R} \int_{\partial\Omega_R} \Gamma_L(r_L, r'_L; \omega) G^r(r'_L, r_R; \omega) \\ & \times \Gamma_R(r_R, r'_R; \omega) G^a(r'_R, r_L; \omega) dr_L dr'_L dr_R dr'_R, \end{aligned} \quad (9)$$

Where G^a is Green's advanced function. Thus one needs the Green's function values only at the boundaries $\partial\Omega_{L/R}$. For a finite bias the electric current is calculated as

$$I = \frac{1}{\pi} \int_{-\infty}^{\infty} T(\omega) (f_L(\omega) - f_R(\omega)) d\omega, \quad (10)$$

where the Fermi functions f_L and f_R are shifted with respect to each other by the bias voltage V_{SD} . In the zero bias limit $f_L(\omega) = f_R(\omega) = f(\omega)$ and one obtains the linear-response conductance

$$G = \frac{1}{\pi} \int_{-\infty}^{\infty} T(\omega) \frac{df(\omega)}{d\omega} d\omega. \quad (11)$$

At zero temperature the conductance is simply $T(\omega_f)$, where ω_f is the Fermi energy. At a finite temperature also electron states with energies near the Fermi level contribute to the conductance, as the derivate of the Fermi function $f(\omega)$ differs from the delta function. A finite temperature influences the solution also through the electron density (cf. Eqs (5) and (6)). Below we show also differential conductances corresponding to given bias voltages. At zero temperature they can be computed from the approximation

$$\frac{dI}{dV_{sd}} \approx \frac{I(V_{sd} + \delta V) - I(V_{sd})}{\delta V} \quad (12)$$

where δV is a small increment in the bias voltage.

We have numerically implemented the non-equilibrium DFT-based scheme using the finite-element method as explained earlier [13]. The size of the matrices to be inverted is determined by the number of the finite-element basis functions needed in the calculations. We have implemented 2D high-order polynomial bases [16] up to the fourth order in order to reduce the basis size. In a typical calculation the number of basis functions ranges from 2800 for to high-order polynomials to 5500 for low-order polynomials.

III. RESULTS AND DISCUSSION

A. Spin polarization in the QW

In this model, there are electronic resonance states in the QW, which are reflected as peaks in the LDOS (see Fig. 7 below). The peaks are broader in short and wide QW's than in long and thin ones, because short QW's are more strongly connected to the electrodes. If the resonance peaks are narrow enough, a spontaneous spin polarization may occur with a spin gap opening between the spin-up and spin-down states below and above the Fermi level, respectively. The polarization occurs in a limited range of gate voltages. At small gate voltages there is no polarization and it disappears again at large voltages. This is in accordance with the density-dependent opening of the spin gap speculated by Reilly *et al.* [4]. A solution with spin polarization in the QW is shown in Fig. 2 which gives the total electron density and the difference between the spin-up and spin-down densities. The electron wave functions have in this case no nodes in the direction perpendicular to the QW, so that there is only a single conducting mode.

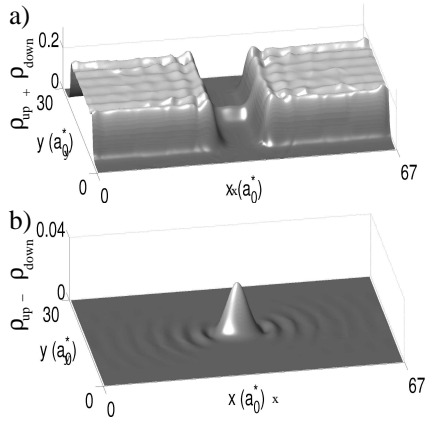


FIG. 2. (a) Total electron density and (b) difference between the spin-up and spin down electron densities at the zero temperature for the system with the dimensions $S=5 a_0^*$, $L=7 a_0^*$, $W=20 a_0^*$, $A=47 a_0^*$ (see Fig. 1) and for the gate voltage $V_g = 12.4$ mV

Berggren and Yakimenko [8] have studied the spin polarization in QW's. In their calculations the electrodes are modeled by two large quantum dots which are connected by the QW. The potential and the electron density inside the QW are controlled by a gate voltage. The electron density is calculated from the wave functions using the DFT within the LDA. They obtain a spin polarization which closely resembles our results. The spread of the polarization in the electrodes is somewhat larger than in our cases which show only a small oscillating polarization outside the QW.

Berggren and Yakimenko do not report on the details of the resonance peaks in the DOS. The resonance state parameters are crucial in the Kondo model. Therefore Meir *et al.* [6] have used the DFT to model the QPC. In their calculations the semi-infinite electrodes are modeled by wires with a parabolic confinement potential perpendicular to the wire axis, and a raise in the external potential forms the QPC as a saddle-point. Due to the different potential construction the resonance peaks obtained by Meir *et al.* are remarkably wider than those in our calculations. A similar QPC construction is used also in the calculations by Hirose *et al.* [18]. The polarizations they obtain are similar to our results for long QW's.

B. Conductance as function of the width of the wire

The conductances of three QW's A, B and C with different widths are shown in Fig. 3 as a function of the gate voltage at zero temperature. The QW's have the same length $L=7 a_0^*$ but for A, B, and C the widths $S=5 a_0^*$, $6 a_0^*$ and $10 a_0^*$, respectively. The staircase quantizations of the conductances are clearly seen. For the widest wire C the perpendicular states are denser in energy than for the thinner wires A and B, so that the conductance steps

are shortest for C. The first plateau for C is also disturbed by the states decaying from the electrodes to the QW. Wires A and B are connected more weakly to the electrodes and for them the first plateau is clearer. A weak connection causes also the spin-polarization in wire A, seen as a short plateau clearly below $1 G_0$. Wire C is not polarized and in wire B the polarization is not strong enough to cause plateaus deviating from integer of G_0 values.

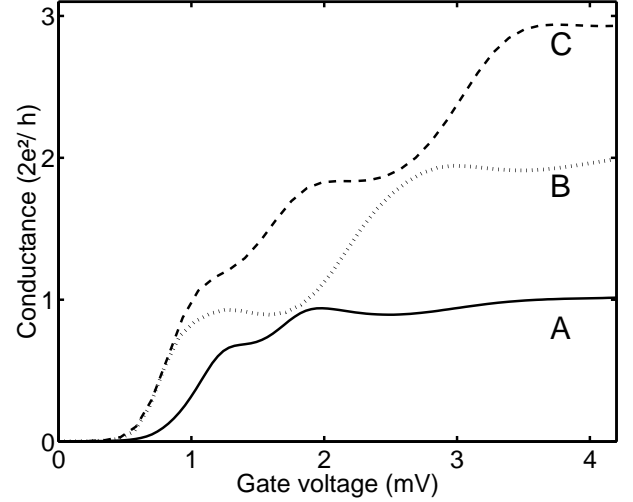


FIG. 3. Conductance at zero temperature as a function of the gate voltage for three wires with the length $L=7 a_0^*$ and widths $S=5 a_0^*$ (A), $6 a_0^*$ (B) and $10 a_0^*$ (C). The width of the electrodes is $W=20 a_0^*$, and the length of the computational area is $A=47 a_0^*$ (see Fig. 1.).

The gate voltage drives the electrostatic potential quite uniformly within the QW. In experiments, side gates are often used to control the potential [1]. These gates not only increase the potential in the QW, but they also make it narrower. The result is a conductance staircase as a function of the gate voltage. The first measured plateaus corresponding to $1G_0$ are pronounced [1] in contrast to our shoulder-like first plateau for wire C. Below we are concerned mainly with the conductance plateaus below $1G_0$ and therefore we discuss wires with the width $S=5 a_0^*$ (wire A in Fig. 3).

C. Conductance as function of the length of the wire

The conductances of the wires with the width $S=5 a_0^*$ and with different lengths L are shown in Fig. 4 as a function of the gate voltage and at zero temperature. The figure shows clearly the effect of the electrode-wire connection. The long wires have clear peaks due to the resonances. The heights of the peaks are $0.5 G_0$, meaning that only a single electron polarized mode contributes to them. The wires with the lengths $L=6...8 a_0^*$ exhibit resonances which are just narrow enough for the spin polarization to appear. The length dependence of the

conductance among these three wires is in qualitative agreement with the recent measurements for QW's by Reilly *et al.* [4], although the wires in the experiments are clearly longer than in our calculations.

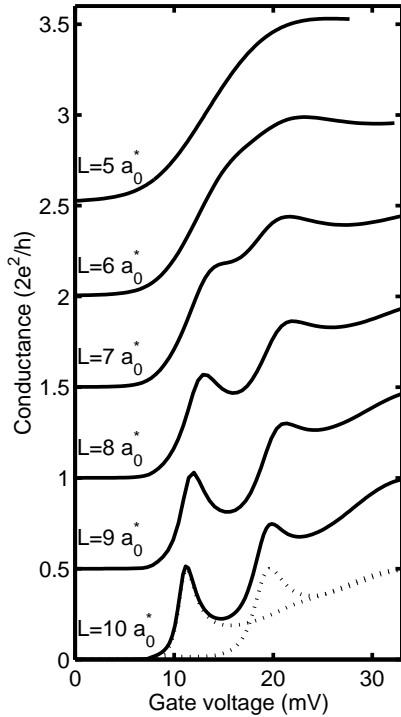


FIG. 4. Conductance as a function of the gate voltage for QW's with the width $S=5 a_0$ and with different lengths L . The width of the electrodes is $W=20 a_0^*$, and the length of the computational area is $A=47 a_0^*$ (see also Fig. 1). The successive curves have been shifted by $0.5 G_0$. The conductance of the wire with $L=10 a_0$ is decomposed into spin-up and spin-down contributions (dotted lines).

Berggren and Yakimenko [8] have also calculated the conductance of their QW system using a rough scheme. They fit parabolic curves to the effective potential in the middle of the QW. The fitting parameters are then used in the Büttiker model for the conductance. The results have the same overall features as ours for the longest wires in Fig. 4, but the changes in the polarization and in the conductance are less abrupt in our calculations. Berggren and Yakimenko argue that the rapid changes are due to the finite-size effects. Therefore our results describing infinite systems seem to support their statement. The conductance-gate voltage curves by Berggren and Yakimenko show two plateaus, one plateau when the polarization appears and another one at $\sim 0.75 G_0$, just before the polarization disappears. This result resembles our curves for the long wire with $L=10 a_0^*$. However, there is a notable difference that in our calculations for the long wires the polarization at low gate voltages is first nearly perfect whereas that by Berggren and Yakimenko is first absent and appears then as a partial polarization. In our conductance curves only one plateau is seen when

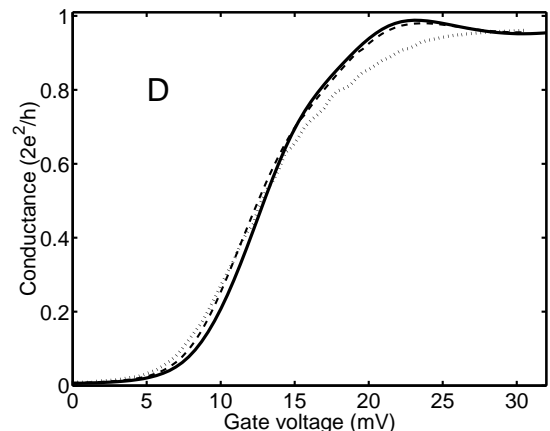
the polarization reaches its maximal value.

D. Temperature dependence of the conductance curves

The effect of the temperature on the conductance behavior of three QPC-like wires D, E and F is shown in Fig 5. At zero temperature, wire D ($L=6 a_0^*$) shows no plateau, whereas wire E ($L=7 a_0^*$) has a plateau at $\sim 0.7 G_0^*$ and wire F ($L=8 a_0^*$) at $\sim 0.5 G_0$. When temperature increases the plateaus below $1 G_0$ in wires E and F shift down wards and become smoother. Wire D shows a weak temperature dependence so that the slope at $\sim 0.7 G_0$ decreases.

Reilly *et al.* [19] have presented a phenomenological model for the appearance and the location of the conductance plateaus. They report on the measurements of three QPC's and explain their conductance behaviors. Two of the QPC's have plateaus at $\sim 0.5 G_0$ and $\sim 0.7 G_0$ and the third one has a very weak plateau at $\sim 0.6 G_0$. The QPC's, D, E and F in Fig. 5 show similar gate-voltage and temperature dependences.

In the model of Reilly *et al.* the relevant parameter is the ratio between the spin gap width and the thermal energy $k_B T$. According to our calculations the temperature broadening in the Fermi functions is small when compared to the resonance peak widths arising from the interactions with the electrodes. Because of this, $k_B T$ has to be replaced by the resonance peak width as the relevant parameter. Then the model can be used to explain the conductance-gate voltage curves also at zero temperature.



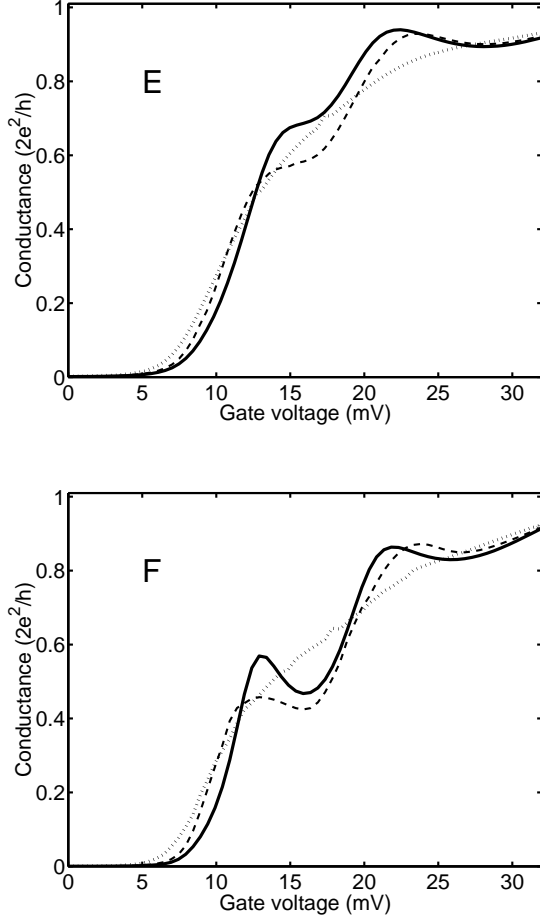


FIG. 5. Conductance as a function of the gate voltage for QW's with the width $S=5 a_0^*$ and lengths $L=6 a_0^*$ (D), $7 a_0^*$ (E) and $8 a_0^*$ (F) at temperatures of 0 K (solid curve), 2 K (dashed curve) and 4 K (dotted curve).

Reilly *et al.* [19] have given three scenarios based on their model. In their scenario I the spin polarization increases rapidly with the increase of the electron density at the QPC. Then a plateau appears at $\sim 0.5 G_0$. This corresponds to our wire F, in which the resonance peaks are narrowest. In the scenario II by Reilly *et al.* the temperature broadenings (the widths of the resonance peaks in our generalization) are comparable to the spin gap. This corresponds to our wire E. When the spin gap begins to open at a certain gate voltage also the spin-down resonance states are partially populated. This situation remains when the density increases and results in the conductance plateau at $\sim 0.7 G_0$. In scenario III by Reilly *et al.* the spin splitting is weak in comparison to the width of the resonance peaks. This corresponds to our wire D for which no plateau is seen at low temperatures.

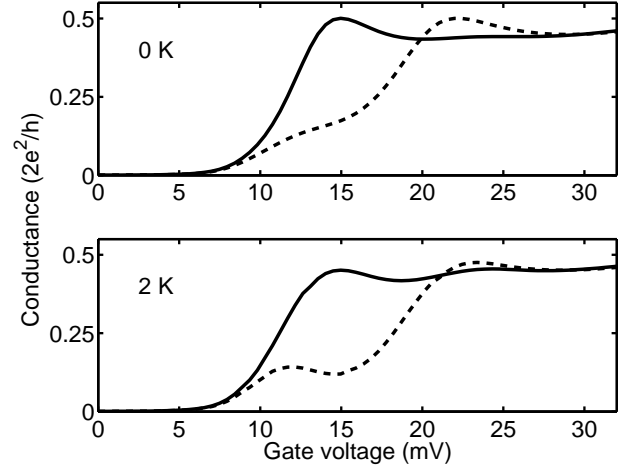


FIG. 6. Conductances due to spin-up (dashed curves) and spin-down (solid-curves) electrons as a function of the gate voltage and at temperatures of 0 K and 2 K. The results are for wire E (Fig. 5) with the length $L=6.5 a_0^*$.

The reason for the different temperature behaviors of the QW's in our model can be seen from the curves in which the conductances caused by spin-up and spin-down electrons are separated. For wire E this is shown in Fig. 6. As temperature increases from 0 K to 2 K spin polarization increases for gate voltages around the middle of the plateau below $1G_0$. At the same time, the resonance peaks also become wider because more states contribute to the conductance (see Eq. (11)). The same behavior is seen also for wires D and F. The reason for the increase in the polarization is seen in the LDOS for wire E in Fig. 7. When the temperature rises the electron density increases in the QW due to the resonances near the Fermi level. Then the decrease in the exchange-correlation energy opens the spin gap, as can be seen in Fig. 7, and the polarization increases. The effect is clearer for wire E than for wires D and F. In wire D the electron density does not increase as fast as in wire E because the resonance peaks are wider. Wire F has a strong polarization already at zero temperature and therefore it cannot show an increase as large as wire E.

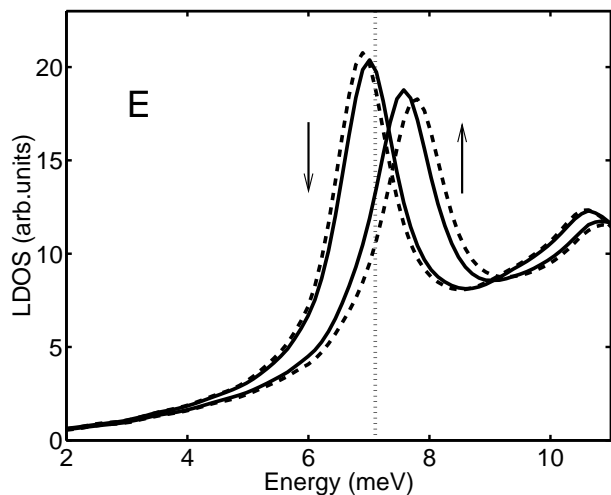


FIG. 7. LDOS corresponding to the QW region (Eq. 8) wire E with the width $S=5 a_0^*$ and length $L=7 a_0^*$. The decomposition to the spin-up and spin-down states at the gate voltage of 14 mV and at the temperatures of 0 K (solid-curve) and 2 K (dashed-curve) are given. The dotted line denotes the Fermi-level.

Meir *et al.* [6] have modeled a QW's using the Kondo model [6] as explained in the Introduction. In their model the Anderson Hamiltonian with parameters controlling the properties of the QPC is used. In their example the conductance plateau is smooth at low temperatures and located around $\sim 0.9 G_0$. As the temperature increases the plateau becomes wider and moves down to $\sim 0.7 G_0$. The behavior is similar to that observed here for wire E.

E. Effect of the bias voltage

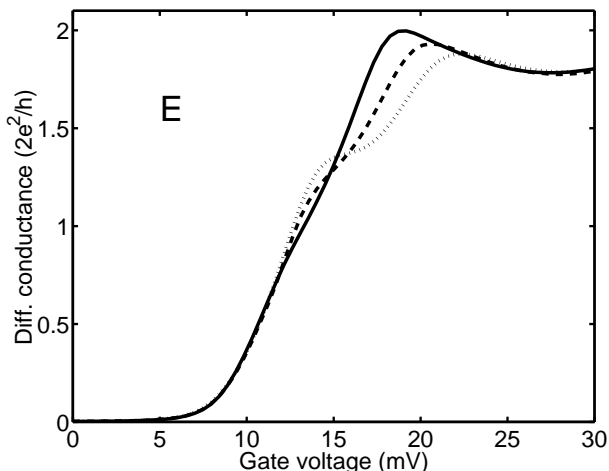


FIG. 8. Differential conductance of wire E with the width $S=5 a_0^*$ and length $L=7 a_0^*$ as a function of the gate voltage and at zero temperature. Results for the bias voltages of 0 mV (dotted curve), 0.23 mV (dashed curve) and 0.46 mV (solid curve) are given.

The differential conductance calculated using Eq. (11) is shown in Fig. 8 as a function of the gate voltage. The increase in the applied bias voltage V_{SD} mainly increases the conductance but at the same time it also curtails the conductance plateaus. This is not exactly in agreement with the measurements which show that the conductance plateau below $1 G_0$ rises with the increasing bias voltage [20,5]. According to our calculations the raise of V_{sd} causes also the decrease in the spin polarization in the QW.

The measured differential conductance suppresses rapidly as a function of the source-drain voltage. This is called as the zero-bias anomaly. Our mean-field model cannot produce this kind of behavior whereas the Kondo model [6] gives an explanation for the zero-bias anomaly. In the Kondo model an unpaired electron couples to the electrons of both leads, resulting in an increased LDOS (Kondo resonance) at the Fermi levels of the electrodes and in an enhanced conductance. When the separation between the Fermi levels increases with bias voltage, electrons can no longer resonantly tunnel through the QPC which leading to the suppression in the conductance.

IV. CONCLUSIONS

We have used the density-functional theory and the Green's function formalism to model electronic transport through ballistic 2D quantum wires. Our results show the appearance of a spontaneous spin polarization in the wire. Under proper conditions, the spin polarization causes a plateau at around $0.7 G_0$ in the conductance as a function of the gate voltage. The calculations explain measurements by Kane *et al.* [1] for the movement of the conductance plateau as function of the wire length. Also the temperature dependence is qualitatively similar to the experimental findings. As a mean-field theory our model can not explain the zero bias anomaly in the conductance. However, the parameters of the resonance state causing the spin-polarization can be used in the Kondo model [5].

ACKNOWLEDGMENTS

We acknowledge the generous computer resources from the Center for Scientific Computing, Espoo, Finland. This research has been supported by the Academy of Finland through its Centers of Excellence Program (2000-2005). P.H. acknowledges financial support by Vilho, Yrjö and Kalle Väisälän foundation.

- [1] B. E. Kane, G. R. Facer, A. S. Dzurak, N. E. Lumpkin, R. G. Clark, L. N. Pfeiffer and K. W. West, Appl. Phys. Lett. **72**, 3506 (1998).
- [2] K. J. Thomas, J. T. Nicholls, N. J. Appleyard, M. Y. Simmpns, M. Pepper, D. R. Mace, W. R. Tribe, and D. A. Ritchie, Phys. Rev. B **58**, 4846 (1998).
- [3] For a review, see *e.g.* C. Joachim, J. K. Gimzewski, and A. Aviram, Nature **408**, 541 (2000).
- [4] D. J. Reilly, G. R. Facer, A. S. Dzurak, B. E. Kane, R. G. Clark, P. J. Stiles, R. G. Clark, A. R. Hamilton, J. L. O'Brien, N. E. Lumpkin, L. N. Pfeiffer and K. W. West, Phys. Rev. B **63**, 121311 (2001).
- [5] S. M. Cronenwett, H. J. Lynch, D. Goldhaber-Gordon, L. P. Kouwenhoven, C. M. Marcus, K. Hirose, N. S. Wingreen, and V. Umansky, Phys. Rev. Lett. **88**, 226805 (2002)
- [6] Yigal Meir, Kenji Hirose, and Ned S. Wingreen, Phys. Rev. Lett. **89**, 196802 (2002)
- [7] D. Goldhaber-Gordon, H. Shtrikman, D. Mahalu, D. Abusch-Magder, U. Meirav and M. A. Kastner, Nature **391**, 156 (1998).
- [8] K.-F. Berggren and I. I. Yakimenko, Phys. Rev. B **66**, 085323 (2002).
- [9] S. Datta, *Electronic Transport in Mesoscopic Systems*, Cambridge University Press (1995).
- [10] T. Morimoto, Y. Iwase, N. Aoki, T. Sasaki, Y. Ochiai, A. Shailos, J. P. Bird, M. P. Lilly, J. L. Reno, and J. A. Simmons Appl. Phys. Lett. **82**, 3952-3954 (2003).
- [11] V. I. Puller and L. G. Mourokh, A. Shailos and J. P. Bird Phys. Rev. Lett. **92**, 096802 (2004).
- [12] Y. Xue, S. Datta and M. A. Ratner, Chemical Physics **281** 151-170 (2002).
- [13] P. Havu, V. Havu, M. J. Puska, and R. M. Nieminen, Phys. Rev. B **69**, 115325 (2004).
- [14] C. Attacalite, S. Moroni, P. Gori-Giorgi, and G. B. Bachelet, Phys. Rev. Lett. **88**, 256601 (2002).
- [15] P. Gori-Giorgi, C. Attacalite, S. Moroni, and G. B. Bachelet, Int. J. Quantum Chem. **91**, 126 (2003).
- [16] Ch. Schwab, *p- and hp-finite Element Methods: Theory and Applications in Solid and Fluid Mechanics*, Oxford University Press (1998).
- [17] The Harwell Subroutine Library, see <http://www.cse.clrc.ac.uk/nag/hsl/>
- [18] Kenji Hirose, Yigal Meir, and Ned S. Wingreen, Phys. Rev. Lett. **90**, 026804 (2003)
- [19] D. J. Reilly, T. M. Buehler, J. L. O'Brien, A. R. Hamilton, A. S. Dzurak, R. G. Clark, B. E. Kane, L. N. Pfeiffer, and K. W. West, Phys. Rev. Lett. **89**, 246801 (2002)
- [20] A. Kristensen, H. Bruus, A. E. Hansen, J. B. Jensen, P. E. Lindelof, C. J. Marckmann, J. Nygård, C. B. Sørensen, F. Beuscher, A. Forchel, and M. Michel, Phys. Rev. B **62**, 10 950, (2000).